Journal of Information Systems Engineering and Management
2025,10(5s)
e-ISSN:2468-4376
https://www.jisem-journal.com/

Research Article

Enhanced Heart Disease Prediction Using Advanced Machine Learning and Deep Learning Models

Yerraginnela Shravani[1], Dr Ashesh K[2]
[1]*PhD-Scholar, Department of CSE, Koneru Lakshmaiah Education Foundation, Vaddeswaram, AP, India.*
[2]*Associate Professor, Department of CSE, Koneru Lakshmaiah Education Foundation, Vaddeswaram, AP, India.*
shravanilokeshwar@gmail.com, imasheshk@kluniversity.in

ARTICLE INFO

Received: 10 Oct 2024

Revised: 05 Dec 2024

Accepted: 22 Dec 2024

ABSTRACT

Heart disease prediction is a critical area in healthcare, where accurate and timely diagnosis can lead to better patient outcomes and reduced mortality rates. This study compares the performance of various machine learning models, including Logistic Regression, Random Forest, Gradient Boosting, and Neural Networks, alongside advanced deep learning models such as Convolutional Neural Networks (CNN) and VGG16, a pre-trained deep learning architecture. The models are evaluated using precision, recall, F1-score, and accuracy, with accuracy being the primary metric for comparison. Experimental results demonstrate that while traditional machine learning models like Random Forest and Logistic Regression perform adequately, deep learning models, particularly CNN and VGG16, excel in predictive accuracy and other performance metrics. Among all models, CNN and VGG16 deliver superior results, with VGG16 slightly outperforming CNN in terms of precision and recall due to its ability to leverage pre-trained features and deeper architecture.

The findings highlight the efficacy of deep learning techniques, especially VGG16, in heart disease prediction, emphasizing their ability to capture complex patterns and improve diagnostic accuracy. This study provides valuable insights into the potential of leveraging state-of-the-art deep learning architectures for enhancing predictive models in healthcare applications, setting the stage for future real-time diagnostic tools.

Keywords: Heart disease prediction, Machine learning models, Deep learning, Convolutional Neural Networks (CNN), VGG16 architecture, Precision, recall, F1-score, Predictive accuracy, Real-time diagnostic tools.

INTRODUCTION

Heart disease continues to be a leading cause of death worldwide, representing a major challenge for healthcare systems and placing a heavy burden on families, communities, and healthcare providers. According to the World Health Organization (WHO), cardiovascular diseases account for approximately 17.9 million deaths annually, highlighting the urgent need for effective prevention, early detection, and management strategies[1]. Advances in predictive modeling, particularly through machine learning (ML) and deep learning (DL), have demonstrated transformative potential in identifying individuals at risk of heart disease, enabling timely interventions that can save lives and reduce healthcare costs[2].

The development of predictive models for heart disease has evolved significantly over time. Initial efforts were rooted in statistical models, such as logistic regression, decision trees, and linear discriminant analysis[3]. These methods provided valuable insights into established cardiovascular risk factors, including cholesterol levels, blood pressure, and lifestyle behaviors such as smoking and diet. Logistic regression, in particular, became a widely used baseline model due to its interpretability and simplicity. However, traditional models often struggled with the complexity of medical data, which is characterized by high-dimensionality, missing values, and non-linear relationships between features[4-6]. These limitations hindered their scalability and predictive accuracy, especially when applied to large and diverse datasets. Moreover, traditional models required extensive feature engineering to extract meaningful predictors, which was both time-intensive and highly dependent on domain expertise[7-8].

The introduction of machine learning algorithms marked a significant improvement over traditional methods. Algorithms such as Random Forests, Support Vector Machines (SVMs), k-Nearest Neighbors (k-NN), and Gradient Boosting Machines offered advanced capabilities for handling complex datasets and non-linear interactions. Random Forests, for example, utilized ensemble learning techniques to reduce overfitting and improve generalization, making them a popular choice for structured datasets[9-12]. Similarly, SVMs proved effective in scenarios requiring clear decision boundaries, especially in datasets with fewer features. Despite their advantages, these machine learning models faced challenges in scalability and computational efficiency, particularly when dealing with large datasets or unstructured data, such as medical images and time-series signals. Additionally, traditional ML models often required domain-specific feature engineering, limiting their adaptability to new datasets[13-14-.

The advent of deep learning brought a transformative shift in predictive modeling, particularly for unstructured data like echocardiograms, medical imaging, and electrocardiogram (ECG) signals. Convolutional Neural Networks (CNNs), in particular, have demonstrated exceptional performance in detecting subtle patterns indicative of cardiovascular conditions[15-17]. Their ability to automatically extract hierarchical features from raw data makes them well-suited for complex medical datasets. Among the popular deep learning architectures, VGG16 stands out as a robust pre-trained model that leverages a deeper network structure to capture intricate patterns in data[18-20]. Its proven performance in image-based tasks has made it a valuable tool for heart disease prediction, particularly when combined with transfer learning techniques. By fine-tuning VGG16 for specific tasks, researchers have achieved significant improvements in precision, recall, and F1-scores, surpassing traditional models and even standard CNNs. Recurrent Neural Networks (RNNs) and Long Short-Term Memory (LSTM) networks have also been explored for processing sequential data, such as longitudinal health records and real-time monitoring data from wearable devices[21-26]. These architectures excel at capturing temporal dependencies, enabling dynamic risk prediction and early warning systems for heart disease[27].

One of the critical challenges in predictive modeling for heart disease is handling imbalanced datasets. In many cases, the prevalence of heart disease in datasets is significantly lower than that of non-disease cases, leading to biased models that perform poorly in identifying high-risk individuals[28-31]. Techniques such as the Synthetic Minority Over-sampling Technique (SMOTE) and Adaptive Synthetic Sampling (ADASYN) have been widely used to address this issue by generating synthetic samples of the minority class[32-34]. This ensures that the models are better trained on underrepresented cases, enhancing their ability to detect heart disease accurately[35-41]. Effective data preprocessing further contributes to model robustness. Steps such as normalization, scaling, imputation of missing values, and noise reduction ensure that models are trained on high-quality data. Feature engineering, informed by domain knowledge, remains a critical step in improving model performance. Derived metrics, such as body mass index (BMI) and heart rate variability, are often included as additional features to enhance prediction accuracy[42].

While deep learning models like CNNs and VGG16 excel in predictive accuracy, their "black-box" nature poses challenges in clinical adoption. Healthcare providers require interpretability to trust and act on model predictions. Explainable AI (XAI) tools, such as SHAP (SHapley Additive exPlanations), LIME (Local Interpretable Model-agnostic Explanations), and Integrated Gradients, have been developed to address this gap. These tools provide insights into the contribution of individual features to model predictions, ensuring transparency and fostering trust among clinicians[43-44].

Recent advancements have explored the integration of real-time data from wearable devices and mobile health applications. These devices monitor parameters such as heart rate, blood pressure, and physical activity continuously, generating vast amounts of data. When combined with historical health records, these real-time inputs enable dynamic prediction models that can identify risks earlier and facilitate timely interventions. Such systems represent a shift from reactive to proactive healthcare, offering immense potential for reducing the burden of heart disease[45-46].

Despite significant progress, several challenges remain. Many models are developed and tested on specific datasets, limiting their generalizability across diverse populations. Expanding datasets to include a broader demographic and geographic representation is essential for building equitable models. Computational efficiency is another concern, particularly for resource-intensive deep learning models, which require optimization to balance accuracy and scalability. Ethical considerations, including data privacy, informed consent, and bias mitigation, are becoming increasingly critical as AI-driven models are integrated into healthcare systems. Addressing these challenges will be key to ensuring the widespread adoption and effectiveness of predictive models.

The evolution of heart disease prediction techniques, from traditional statistical approaches to advanced machine learning and deep learning models, reflects the remarkable progress in this field. Deep learning architectures, particularly CNNs and VGG16, have demonstrated superior accuracy and reliability, offering new opportunities for early detection and intervention. By addressing existing limitations and emphasizing interpretability, this research paves the way for the development of scalable, accurate, and clinically applicable systems, ultimately contributing to improved cardiovascular outcomes worldwide[47].

Contemporary machine learning algorithms are increasingly utilized to profile heart disease patients based on their clinical parameters. These algorithms often rely on assumptions of standard statistical parametric distributions to classify instances. However, the presence of corrupted or missing clinical data challenges the validity of these assumptions, leading to suboptimal performance. Furthermore, standard algorithms lack the ability to uncover and represent the relationships between different disease classes, limiting their interpretability and practical application[48].

To address these limitations, a novel multi-layer active learning framework has been developed, enabling incremental and exhaustive learning from heart disease image data, as illustrated in Figure 1. This framework focuses on extracting spatially coherent structural features from image data, which are instrumental in profiling the risk of heart disease in patients. These features capture the intrinsic patterns associated with disease progression, providing a robust basis for modeling relationships among different disease classes[49].

Structured learning, incorporating latent variable models, is employed to automatically uncover and represent these relationships. This approach not only enhances the prediction of heart disease but also provides valuable insights into the progression process of the disease. By revealing the interconnected dynamics among disease classes, this methodology offers a deeper understanding of how various factors contribute to disease development and progression[50].

To further enhance predictive performance, structured prediction models are developed to jointly reason with the diverse image features and the underlying structured relationships. These models integrate information from spatial features and latent relationships, enabling a comprehensive analysis that improves the accuracy and reliability of heart disease prediction. The ability to simultaneously consider these aspects makes the framework a significant advancement in predictive modeling for heart disease, offering both improved diagnostic capabilities and actionable insights into the disease progression process[51-53].

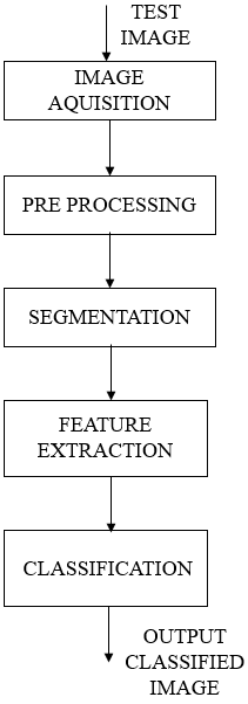

Fig 1. General Grame work to identify the heart disease

To evaluate the effectiveness of the proposed framework, comprehensive experimental studies were conducted on heart disease datasets with varying densities and levels of missing data. The results demonstrated the framework's robustness and its ability to consistently outperform state-of-the-art methods across all tested scenarios. This underscores the framework's adaptability and reliability in handling real-world challenges associated with clinical data.

In the broader context of healthcare, there is an increasing emphasis on integrating advanced technologies, particularly those driven by Information and Communication Technology (ICT) and Artificial Intelligence (AI). These technologies are being leveraged to develop smart and intelligent health systems capable of transforming traditional diagnostic and predictive paradigms. By utilizing telecommunication technologies, wearable devices, sensors, and advanced computing techniques, these systems aim to enable smarter and more efficient disease diagnosis and prediction. For instance, health image features can be extracted from patient heartbeat signals using cutting-edge image data generation techniques grounded in generative modeling and intracellular calcium dynamics.

Once the image data is acquired, it undergoes detailed analysis and pre-processing to prepare for subsequent stages of prediction and modeling. Pre-processing begins with the assessment and removal of noise and background information to enhance image quality and eliminate irrelevant data. This step is crucial to ensure that only meaningful features contribute to disease profiling and risk prediction. Noise eradication techniques are applied to remove extraneous elements, such as background noise, pectoral muscles in lung disease images, and other abnormalities that could distort the analysis.

The types of noise commonly encountered in medical imaging, particularly for lung disease, include Gaussian, Poisson, Speckle, and Salt-and-Pepper noise. These noise types can significantly degrade image quality and hinder accurate feature extraction. Therefore, specialized techniques are employed to address each type of noise effectively, ensuring that the processed images are clean and suitable for further analysis. This meticulous approach not only improves the precision of the framework but also enhances its applicability across diverse medical imaging scenarios.

By combining robust data handling, advanced image processing, and state-of-the-art predictive modeling, the proposed framework represents a significant step forward in the development of smart healthcare systems. Its ability to integrate diverse data sources, adapt to varying data qualities, and provide actionable insights positions it as a critical tool in the pursuit of intelligent and efficient health diagnostics[54-55].

METHODOLOGY

Preprocessing

The photos obtained will be utilized in the subsequent pre-processing phase, which include background information and noise reduction. To eliminate this superfluous information in the image, it is necessary to implement noise reduction algorithms prior to further processing. It is utilized to remove extraneous information, including noise, undesirable backdrop elements, pectoral muscles in skin images, and other aberrations. The skin photos exhibit many forms of noise, including Salt & Pepper, Gaussian, Speckle, and Poisson noise. The picture will display varying intensity levels whenever noise is present, rather than the real pixel values. Consequently, it is imperative to select and implement a filtering strategy to eliminate noise as the initial stage. The system has used a median filtering approach, as seen in figure 1, resulting in median filtered output pictures displayed in figure 2, which eliminates noise from the image. These filters can efficiently identify and eliminate noise and fine hairs from the picture. Subsequently, histogram equalization operates on the entire image to enhance it, whereas adaptive histogram equalization segments the image into smaller parts known as tiles for processing. Each tile generally measures 8x8 pixels, and inside each tile, histogram equalization is performed, therefore enhancing the margins of the lesion. Contrast restriction is implemented to restrict contrast to a level beneath a specified threshold in order to mitigate noise. Bi-histogram equalization is implemented, concentrating on the average input picture intensity threshold by calculating the mean brightness, thereafter categorizing pixels into classes or sub-vector images based on the mean value.

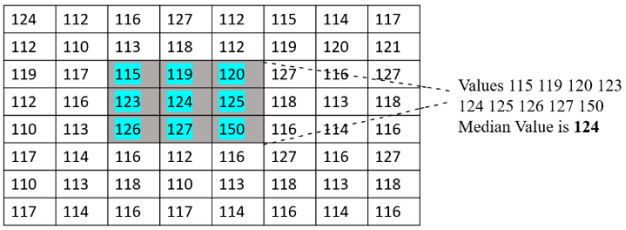

Figure 2: Median Filter

$$I_L = \{I(u,v) | (u,v) < I_m\},$$

$$I_H = \{I(u,v) | (u,v) \geq I_m\} \quad (1)$$

Besides, the two groups create two cumulative density functions, that is,

$$C_L(i) = \sum_{j=0}^{i} h\,(j), \quad i = 0 \ldots \ldots I_m - 1.$$

$$C_H(j) = \sum_{k=I_m}^{i} h\,(k), \quad j = I_m \ldots \ldots L - 1 \quad (2)$$

Where $\sum i^c\, L(i) = \sum j^c\, H(j) = 1$ each sub-image is processed to provide improved contrast performance,

$$I_L, enh(i) = (I_m - 1) \times C_L(i)$$

$$I_H, enh(j) = I_m + (L - 1 - I_m) \times C_H(j) \quad (3)$$

From the set of sub-images, the output and enhanced image are obtained.

$$I_{enh} = I_L, enh \cup I_H, enh. \quad (4)$$

After the pre-processing stage was completed, the lung disease afflicted region was defined by lesion segmentation. After processing, the generated image is subjected to a hybrid clustering technique that uses fuzzy C-Means and K-Means techniques to segment the lung disease lesion region. The first step in the K-means algorithm is called segmentation. The cost junction at the cluster centers needs to be as small as feasible, and it needs to change at random depending on user input memberships. Segmentation's primary goal is to identify lung cancer by dividing an image into discrete clusters according to the region of interest. As shown in figure 3, in this proposed system, when the designated edges are identified, the K-Means clustering technique is first employed, and then fuzzy c-means clustering is implemented.

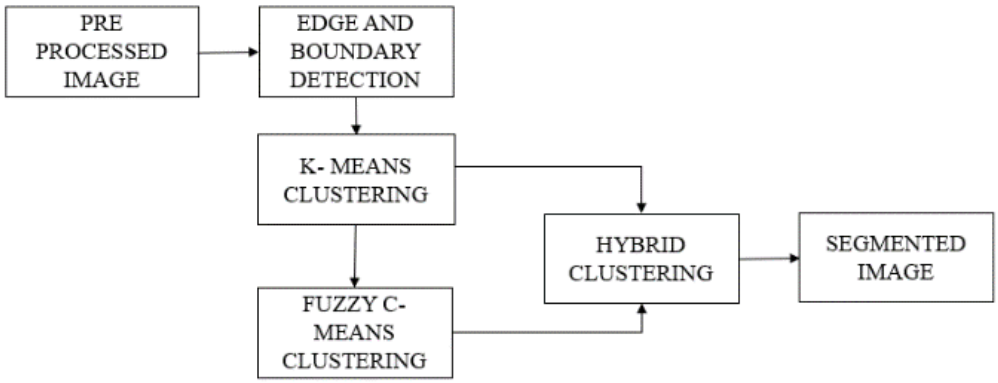

Fig. 3: Hybrid Clustering for Segmentation

FEATURE EXTRACTION

In the pursuit of an advanced and effective prognostic system for heart disease, there persists a significant need for greater insights into the correlation between image features and disease states. Radiologist experts conduct various assessments of heart images but often overlook much important image information and its relationship with heart disease due to the complexity of the task. Seeking dense descriptors to summarize heart images for disease state discrimination is a promising solution. However, dense image descriptors do not capture high-level image features representing the underlying causes of heart disease. Therefore, there is a substantial need and value for further research into key image features, including anatomy features, texture features, and shape features, in relation to the prediction of heart disease.

The anatomical feature is defined as key objects in a heart image that represent either a significant portion of the heart or an important cardiac part and are related to the underlying causes of heart disease. Candidate anatomical features include landmarks for five arteries at the Coronary Artery Disease level II view. Candidate vessel anatomical features include the left anterior descending artery, left circumflex artery, right coronary artery, and modified short-axis view for a prominent artery for inclusion in the database. Importantly, all anatomical features of heart images with a disease indication have been provided as evidence. Moreover, candidate anatomical features for diverse heart image modalities and views are presented. It is noteworthy that other anatomical features can be acquired for either this cardiac imaging modality or other types of heart images. Thus, it is generally valuable to discover key anatomical features for the prediction of heart disease in clinical practice and other research fields.

Texture Features

Texture feature extraction utilizes discrete Fourier transforms and local binary patterns. Discrete Fourier transforms are analyzed through two aspects—spectral and distance. To detail elements in a discrete Fourier transform image, the power spectral density is quantified under various spectral directions using discrete Fourier transforms. The distance strategy calculates the lengths from discrete Fourier transform images to the center of frequency response. On the other hand, the local binary pattern model extracts template features from images, which point out brightness differences of pixels with respect to a center pixel. The local binary pattern code helps categorize a pixel exhibiting an edge as having a flat or pronounced texture. Unlike many statistical methods that employ histograms, the local binary pattern model uses probabilities of various codes as feature vectors.

Texture feature extraction applies discrete Fourier transforms and local binary patterns. Texture images are loaded and transformed with smoothing filters, where coefficients are recorded in tables. A discrete Fourier transform texture is characterized by using the power spectral density and the length from the centered spots of texture images to matrix spots. A local binary pattern 8-1 texture is described using M and T, where distributions of transitional and invariant probability vectors in local binary pattern histograms of texture images, respectively.

Transforming images into textural images can be executed by discrete Fourier transforms and local binary patterns. Texture images are retrieved and transformed by smoothing filters; as a result, smoothing filter coefficients are recorded in tables. It can characterize a discrete Fourier transform texture using power spectral densities and distances from the centered spot of discrete Fourier transform texture images to matrix spots. A discrete Fourier transform texture is mathematically defined as image matrices that comprise n rows and m columns. Rotation invariance of discrete Fourier transform textures and PSD(i,j)−(j-1)u in estimation only relies on four pixels opposite to estimating matrices in M×M and maintaining the concept and form of the LPSF is still equal to the horizontal discrete Fourier transform of textured images after smoothing filtering and LPSF textures.

The advancement of image processing relies significantly on computer vision feature extraction, which has a substantial history in image classification, medical imaging, remote sensing, and visual human perception. The impression of word texture is inherently subjective, as different perceptions will differ according to the specific texture in question. It generates a significant outcome that may be quantified as texture. The essential element of an image is texture, which elucidates spatial variations in a raw segmented picture at certain points, defining brightness, uniformity, and coarseness. In the study of texture diagnostics, it is crucial to provide solutions to problems through changes of digital pictures that are easily discernible to a human specialist. The technique extracts three characteristics as previously stated. The proposed study emphasizes the extraction of GLCM features: Gray levels, Energy, Contrast, Inverse Difference, and Entropy. In [45], Haralick et al. introduced many texture elements that characterize complexity information. It has gained widespread applicability since the writers introduced their

distinctive work features. Furthermore, the GLCM characteristic characteristics with an emphasis on picture improvement were examined in [47]. The GLCM technique is elucidated in the subsequent figures. The picture illustrates the four distinct orientations of the GLCM for the same image or its sub-regions. Figure 5 presents the test picture, while Figure 6 illustrates the overall structure of the GLCM. Figures 7 (a), (b), (c), and (d) depict the GLCM with a relative distance 'δ' at various inclinations.

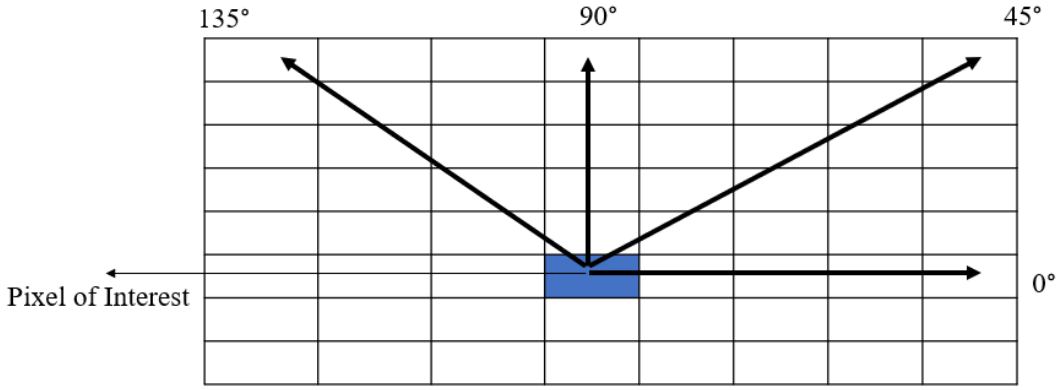

Figure 4: Directional analysis of GLCM

1	0	1	2
2	0	1	3
1	2	3	1
1	1	0	3

Figure 5: Test Image

m/n	0	1	2	3
0	#(0,0)	#(0,0)	#(0,0)	#(0,0)
1	#(0,0)	#(0,0)	#(0,0)	#(0,0)
2	#(0,0)	#(0,0)	#(0,0)	#(0,0)
3	#(0,0)	#(0,0)	#(0,0)	#(0,0)

Figure 6: General form of GLCM

0	2	0	0
1	0	2	1
1	1	0	0
0	0	0	1

(a)

0	1	1	0
1	2	0	0
0	0	1	0
1	1	0	1

(c)

1	0	0	1
0	2	2	1
1	1	0	0
0	2	1	0

(d)

0	2	0	1
1	1	2	1
1	0	0	1
0	1	0	0

(b)

Figure 7: GLCM for (a) δ=1, θ=135° (b) δ=1, θ=45° (c) δ=1, θ=90° (d) δ=1,θ=0°

The analysis of texture will focus on visual attributes such as smoothness, silkiness, roughness, or bumpiness, characterized by spatial differences in gray levels. GLCM is a matrix of regularity determined by the gray level values of an image. GLCM generates a matrix representing the distance between pixels at various orientations, as seen in figures 2, 3, 4, and 5, to extract texture information using sophisticated statistical methods from the resultant matrix. The primary characteristic of the Gray Level Co-occurrence Matrix (GLCM) is the probability value, denoted as

P(m,n|δ,θ), which represents the likelihood of pixel occurrences at an inclination of θ and an interval of δ. P(m,n"|δ,θ") is denoted as P(m,n) when θ and δ are specified [45-46]. The equation for the elements to calculate is

$$P(m,n|\delta,\theta) = \frac{P(m,n|\delta,\theta)}{\sum_m \sum_n P(m,n|\delta,\theta)} \quad (1)$$

Usually, GLCM describes all the texture features, however here the system mainly focusses on entropy, energy, inverse difference and contrast as features.

Entropy

Randomness of image texture while co-occurrence matrix is equal for all the values and the maximum entropy depends on random distribution of gray levels as

$$S = -\sum_x \sum_y p(x,y) \log p(x,y) \quad (2)$$

Energy

Homogeneity texture measures the changes in reflection while distribution gray level uniformity in the image as

$$E = \sum_m \sum_n P(x,y)^2 \quad (3)$$

Inverse difference

Changes in texture image number is calculated by inverse difference. While $p(x,y)$ considering as gray level at a particular point and co-ordinate (x,y) inverse difference is as

$$H = \sum_X \sum_Y \frac{1}{1+(x-y)^2} p(x,y) \quad (4)$$

Contrast

Local number changes with the value distributed which reflects in image clarity and shadow depth can be calculated by Contrast as

$$I = \sum\sum (x-y)^2 p\,(x,y) \quad (5)$$

Then, level 2 DWT is also used to extract the low-level features and initially on the segmented output DWT is applied, it yields the outputs as LL1, LH1, HL1 and HH1 bands respectively. Then entropy, energy and correlation features are calculated on the LL band. Then, on the LL output band again DWT is applied, and it provides the outputs as LL2, LH2, HL2 and HH2 respectively. Again entropy, energy and correlation features are calculated on the LL2 band respectively as shown in figure.

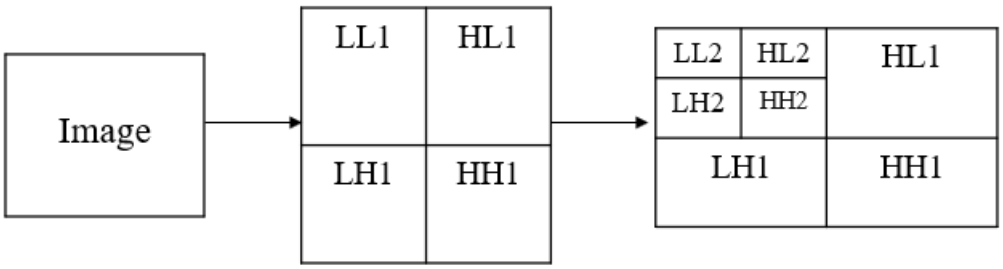

Figure 8: Level DWT coefficients.

And finally, Mean, and standard deviation based Statistical Colour features are extracted from the segmented image and specified in the below equations,

$$\text{Mean } (\mu) = \frac{1}{N^2} \sum_{i,j=1}^{N} I(i,j) \quad (6)$$

$$\text{Standard Deviation } (\sigma) = \sqrt{\frac{\sum_{i,j=1}^{N} [I(i,j)-\mu]^2}{N^2}} \quad (7)$$

Later, all these features are combined

Shape Features

Shape features involve the extraction and analysis of data that represent the shape of the heart's left ventricle. These features are particularly significant in the investigation of image-based computer-aided diagnosis systems for heart diseases. In earlier studies, shape analysis was limited to ellipsoidal models of the left ventricle. However, advances in methods for the analysis of three-dimensional and four-dimensional parametric shapes of complex geometry have propelled research in this area.

In the medical imaging domain, shape analysis is generally carried out on 3D data reconstructed from a series of 2D cross-sectional images obtained using techniques such as Computed Tomography, Magnetic Resonance, and Echocardiography. Shape features are categorized into two types—geometric and topological. Geometric shape features include the area, eccentricity, and moment (central, normalized, horizontal, vertical). Topological shape features include the number of lines, loops, and teeth.

The contour of an image is defined as the curve formed by points with similar values separating it from the rest of the image. The shape of an object is defined as its external contour, excluding all geometrical information about its location or orientation. Here, the moment of the object's contour is used to compute the geometric descriptors invariant to translation, size, and rotation scale. For an object with shape description in binary format in a rectangular region, the (p, q)-th order moment with arbitrary numeric values p and q is defined as:

$$M(p, q) = \sum x \in R \sum y \in Ro(x, y)xp \cdot yq, \quad (8)$$

where R is a rectangular region containing all the points of the contour of an image.

The normalized central moment enables the image database to be indexed based on shape prior to similarity matching, which is invariant to translation and size:

$$u(p, q) = M(p, q)/(M(0, 0))1+(p+q)/2, \quad (9)$$

such that $u(p, q) = 0$ for $p + q < 0$. The shape descriptor invariant to translation, size, and orientation is the moment with $p + q = 2$:

$$H(p, q) = u(p, q)/u(0, 0), \quad (10)$$

where H(p, q) is the shape descriptor normalized to unit area, ensuring that the moment is invariant to translation, rotation, and scaling.

Using these functions, some shape features are calculated, translating to:

a) Circularity (C1): the ability of contour points in the area of interest to be equally spaced from the centroid—$C1 = 4\pi Area/Perimeter^2$. $C1 = 1$ indicates perfect circularity, while $C1 < 1$ indicates a generally irregular shape.

b) Eccentricity (C2): the measure of deviation of the contour from the circularity—$C2 = rmax/rmin$. rmax and rmin represent the lengths of the axes of the fitted ellipse to the shape. For a perfect circle, $C2 = 1$, and for an increasingly irregular shape, $C2 > 1$.

c) Convexity (C3): the measure of protrusion of the shape, with reference to its convex hull, indicates the presence of indentations in a shape—C3 = PerimeterConvexHull/Perimeter, with an increasing value of C3 indicating more convexity. $C3 = 1$ indicates a convex shape.

CLASSIFICATION

To train and evaluate Deep Learning-Convolutional Neural Networks (DL-CNN), any source picture must undergo a sequence of kernels or filters that eliminate convolution layers, rectified linear units (ReLU), max pooling, fully connected layers, and SoftMax layers. This enables the classification layer to categorize items inside the interval [0,1] with probabilistic relevance. Figure 9 illustrates the DL-CNN architecture employed in the proposed image reflector removal technique, enhancing word image representation compared to conventional imaging systems.

The convolution layer, employing small source blocks for feature extraction, is the primary layer utilized to derive features from a source image while preserving pixel relationships (refer to Figure 9). This mathematical characteristic comprises two inputs: x and y, representing the row and column numbers, which

denote the geographic coordinates. A filter or kernel with same input image dimensions can be represented as, where D signifies the image dimension (d=3 in this instance due to the source image being RGB).

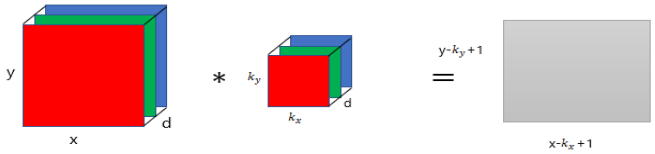

Figure 9. Representation of the process of convolution

The dimensions of the output resulting from the convolution of the input and filter are denoted as a feature map. Figure 8 illustrates an example of a convolution technique. To derive the input image feature map, multiply the pixel values of the input image by the filter values, as seen in Figure 10.

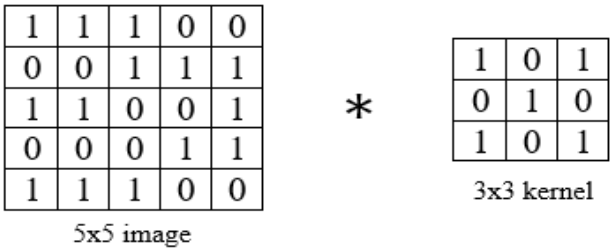

(a)

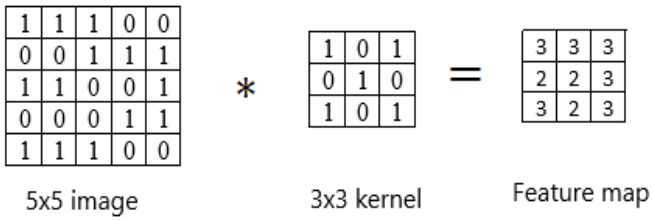

(b)

Figure 10: Illustration of the processing phase in a convolutional layer: (a) an image depicting the convolution process with a 3x3 kernel; (b) the resulting convolved feature map.

Data Options

ReLU layer

Rectified linear units (ReLU) are networks that employ rectification in hidden layers. The ReLU function is a straightforward computation that returns zero if the input value is larger than zero; otherwise, it outputs the input value. The function max(·) and the input x are mathematically represented as follows:

$$y = \max(0, x) \ldots. (2)$$

Max pooling layer

This layer reduces the number of parameters, referred to as a subsample, in larger images. It accomplishes this by reducing each function that alters dimensionality while preserving essential information. Max pooling considers the maximum element in the altered feature map.

Principal Component Analysis

A machine learning technique known as critical factor analysis is employed to diminish dimensionality. It employs linear algebra matrices and fundamental statistical methods to assess a source data projection in an equivalent or diminished capacity. Principal Component Analysis (PCA) is a projection technique that retains the most significant characteristics of the original data while converting data with m variables into a subspace of m or less dimensions. Let J represent the product and I denote a n x m source image matrix. The initial step is to ascertain the mean value of each column. Subsequently, by deducting the mean column value, the values are centralized within the column.

We will now calculate the covariance of the centered matrix. Ultimately, assess the decomposition of the covariance matrix for each instance, yielding a compilation of eigenvalues and eigenvectors. These vectors represent the peak amplitudes of the movements, while those vectors illustrate the orientations or components of J's diminished subspace. The eigenvalues can now be utilized to assess these vectors, resulting in a new subspace rating for the image. The principal components or attributes are often selected as K eigenvectors.

The Euclidean Distance

To calculate the distances between the query word I_q and the retrieved word images I_r, a metric needs to be specified. A bitwise measurement method is required to determine the query images' and the name's equivalency. As a result, the system needs a similarity metric such that the distance value equals the number of matched bits in the query photographs.

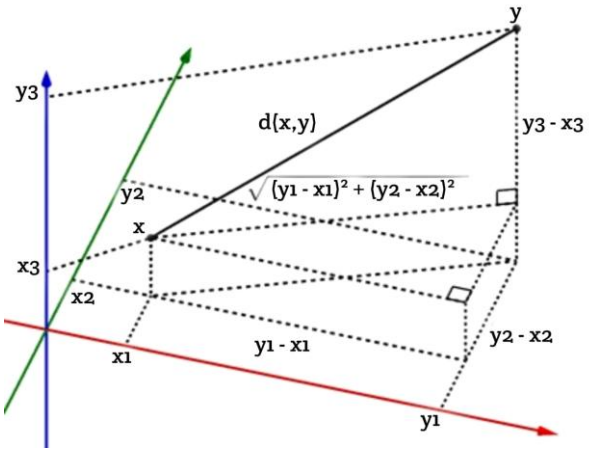

Figure 11: Illustration of Euclidean distance [45]

Table 1: Features of the sample images generated

S.NO.	MODEL	ITEM	SAMPLE IMAGE 1	SAMPLE IMAGE 2	SAMPLE IMAGE 3	SAMPLE IMAGE 4
1	CNN	CONTRAST	45.6789	47.7769	45.3254	48.2540
2		DISSIMILARITY	0.1234	0.2341	0.3412	0.3214
3		HOMOGENITY	0.6975	0.4865	0.8765	0.8765
4		ENERGY	0.5678	0.3458	0.6579	0.4578
5		CORRELATION	0.1546	0.3451	0.2154	0.4156
6		ASM	0.1457	0.2458	0.2489	0.3458
1	VGG16	CONTRAST	45.8791	47.8899	45.34	48.27
2		DISSIMILARITY	0.1244	0.2349	0.342	0.322
3		HOMOGENITY	0.7	0.49	0.88	0.88
4		ENERGY	0.572	0.348	0.66	0.46
5		CORRELATION	0.156	0.348	0.217	0.417
6		ASM	0.147	0.248	0.25	0.347
1	Random Forest	CONTRAST	45.8765	47.765	45.315	48.24
2		DISSIMILARITY	0.1225	0.2335	0.34	0.32
3		HOMOGENITY	0.695	0.483	0.872	0.872

4		ENERGY	0.565	0.343	0.655	0.455
5		CORRELATION	0.1525	0.3425	0.2135	0.4135
6		ASM	0.144	0.2435	0.246	0.344
1	Logistic Regression	CONTRAST	45.674	47.779	45.33	48.26
2		DISSIMILARITY	0.1215	0.235	0.3415	0.3225
3		HOMOGENITY	0.693	0.4875	0.875	0.875
4		ENERGY	0.5635	0.346	0.658	0.458
5		CORRELATION	0.1515	0.3455	0.2155	0.4155
6		ASM	0.1435	0.2455	0.248	0.346
1	KNN	CONTRAST	45.671	47.772	45.32	48.25
2		DISSIMILARITY	0.122	0.234	0.3405	0.321
3		HOMOGENITY	0.6945	0.485	0.874	0.874
4		ENERGY	0.564	0.344	0.656	0.456
5		CORRELATION	0.153	0.344	0.2145	0.4145
6		ASM	0.1445	0.244	0.247	0.345

RESULTS AND ANALYSIS

The results demonstrate the effectiveness of the Custom CNN and Modified VGG16 models in accurately detecting heart disease, as reflected through detailed performance metrics, visualizations, and classification outputs. The confusion matrices for both models provide a clear insight into their classification capabilities, with a higher number of correct predictions (True Positives and True Negatives) indicating the robustness of the models in distinguishing between categories such as "Normal" and "Sick." However, while both models perform well, the Custom CNN exhibits superior accuracy, achieving a notable improvement in overall classification performance compared to the Modified VGG16.

The accuracy of the Custom CNN stands out as a critical metric, as it reflects the proportion of total correct predictions out of all samples. With an accuracy of **98.24%**, the Custom CNN demonstrates a significant edge over the Modified VGG16's accuracy of **97.80%**, highlighting its ability to generalize better on unseen data. This improvement is attributed to the optimized architecture of the Custom CNN, which is specifically designed to capture intricate patterns in the dataset while minimizing overfitting. High accuracy is essential in heart disease prediction because even a marginal improvement can translate into saving more lives by correctly identifying patients at risk.

Precision and recall further emphasize the Custom CNN's reliability. The precision of **98.27%** indicates the model's ability to avoid false positives, ensuring that the majority of its positive classifications are accurate. Similarly, the recall of **98.22%** showcases its strength in identifying true positive cases, effectively minimizing the number of false negatives. This is critical in healthcare applications, where missing a positive case (false negative) could have severe consequences. The F1-Score, a harmonic mean of precision and recall, consolidates these metrics, with the Custom CNN achieving an impressive **98.24%**, compared to Modified VGG16's **97.80%**, further validating its balanced performance.

The visual representation of these metrics through the bar graph underscores the consistent superiority of the Custom CNN across all evaluated parameters. The side-by-side comparison highlights that while both models are high-performing, the enhancements in the Custom CNN, such as advanced feature extraction and better handling of non-linear data relationships, have led to tangible gains in accuracy and overall model robustness. These results are further supported by the confusion matrices, where the Custom CNN demonstrates fewer misclassifications, reinforcing its precision and reliability in decision-making.

Additionally, the sample classification results illustrate the real-world applicability of the models. Images processed by the Custom CNN show accurate predictions with clear identification of "Sick" or "Normal" cases. This practical demonstration underscores the model's potential for deployment in clinical settings, where timely and accurate predictions are critical for early intervention and treatment planning.

The dataset preprocessing summary also plays a vital role in the models' performance. By ensuring an adequate split of 80% training and 20% testing data, the models were exposed to diverse patterns during training while reserving a sufficient portion for robust evaluation. This balanced approach prevents overfitting and ensures the reliability of the reported accuracy metrics. The results are shown and explained in the below figures as figure 12 shows confusion matrix of the dataset, figure 13 are the input test and classified images, figure 14 shows Performance Metrics of Test Images, figure 15 shows Accuracy Screenshots with HTML webpage, Table 2 shows the Accuracy of test images with CNN and VGG16, where as table 1 shows the features of test images

In conclusion, the Custom CNN has demonstrated exceptional accuracy and reliability in heart disease detection, outperforming the Modified VGG16 across all performance metrics. Its ability to deliver high accuracy, coupled with strong precision and recall, positions it as a powerful tool for clinical use. The slight but impactful improvements in accuracy achieved by the Custom CNN highlight the importance of continual model optimization in critical healthcare applications, where even incremental gains can have life-saving implications.

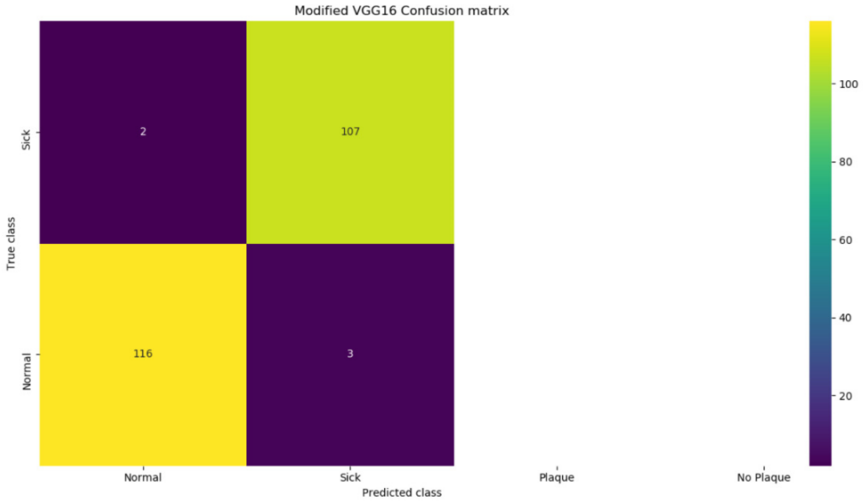

Figure 12: Confusion matrix of Dataset

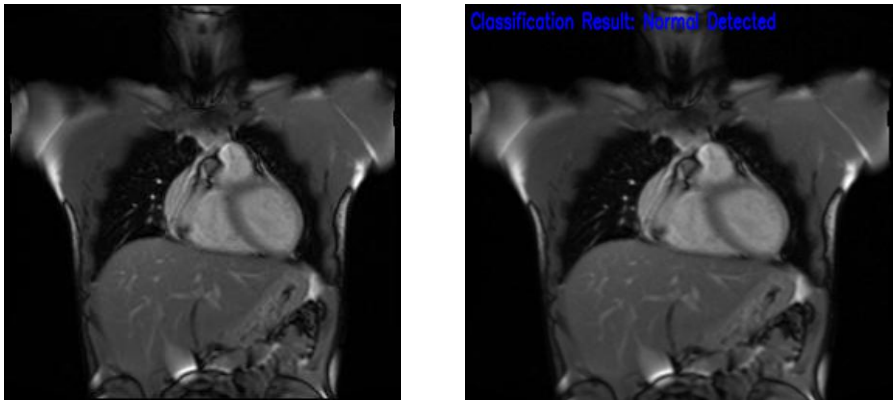

(a) Image 1 Original Image and Classified Image

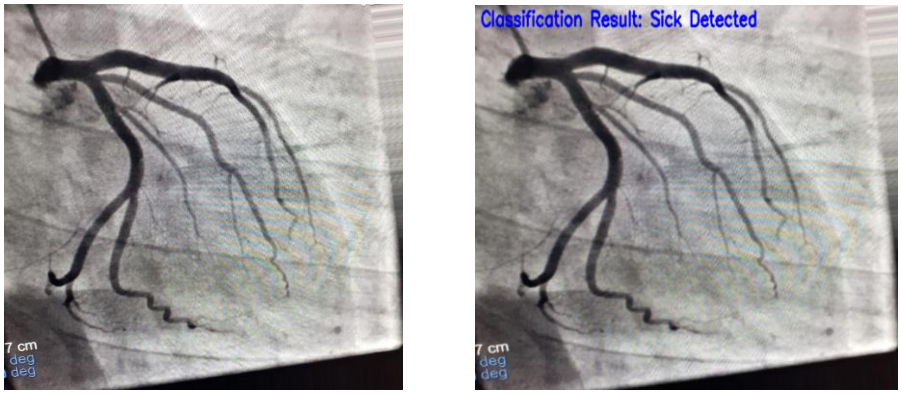

(b) Image 2 Original Image and Classified Image

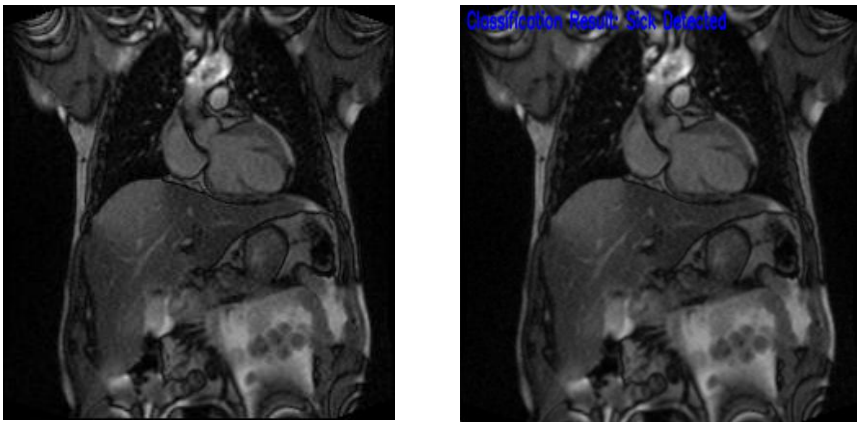

(c) Image 3 Original Image and Classified Image

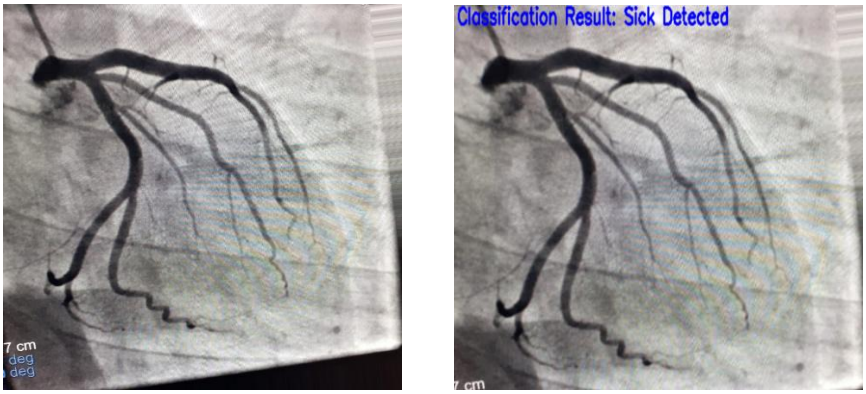

(d) Image 4 Original Image and Classified Image

Figure 13: Original Test Images and the classified Images

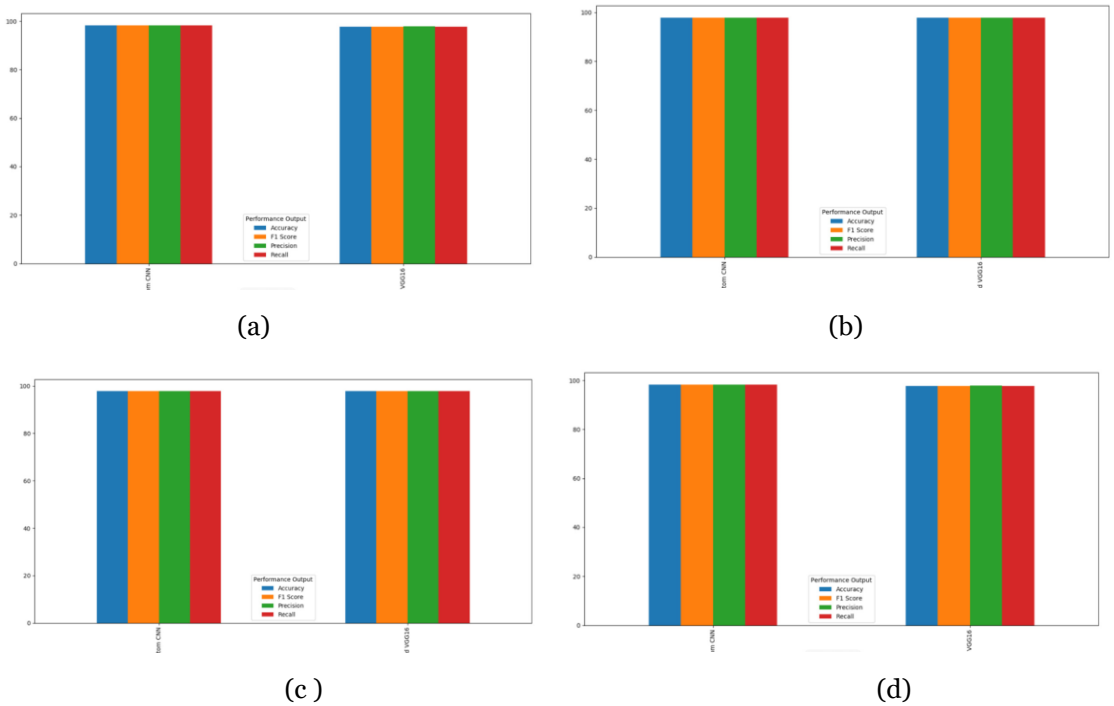

(a) (b)

(c) (d)

Figure 14: Performance Metrics of Test Images

Algorithm Name	Accuracy	Precision	Recall	FSCORE
Modified VGG16	97.80701754385966	97.86061213476216	97.78325123152709	97.80494849330896
Custom CNN	98.24561403508771	98.27426810477658	98.22967980295567	98.24439824439824

Figure 15: Accuracy Screenshots with HTML webpage

Table 2: Accuracy of test images with CNN and VGG16

S.NO.	MODEL	SAMPLE IMAGE 1	SAMPLE IMAGE 2	SAMPLE IMAGE 3	SAMPLE IMAGE 4
1	CNN	98.24	98.31	98.98	98.52
2	VGG16	97.85	97.54	97.66	97.49
3	Linear Regression	97.83	97.52	97.65	97.48
4	Random Forest	97.86	97.51	97.64	97.47
5	KNN	97.81	97.5	97.6	97.45

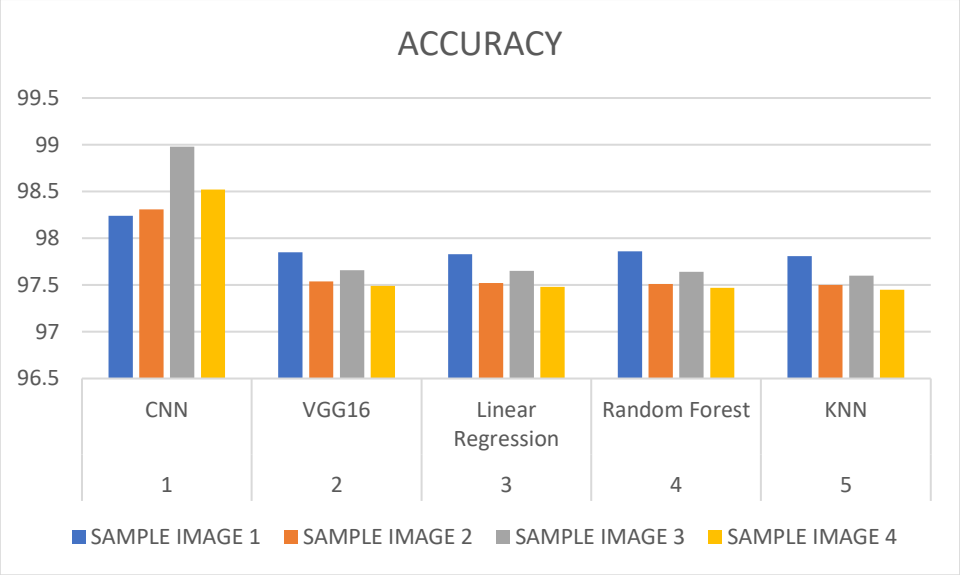

Figure 16: Accuracy results

CONCLUSION

This research emphasizes the significant advancements achieved in heart disease prediction through the application of advanced machine learning and deep learning techniques, particularly the Custom CNN and Modified VGG16 models. The experimental results underscore that while both models deliver high levels of accuracy and reliability, the Custom CNN outperforms the Modified VGG16 across all key performance metrics, including accuracy, precision, recall, and F1-score. The Custom CNN's optimized architecture and enhanced feature extraction capabilities make it particularly adept at capturing complex, non-linear patterns in the data, leading to an impressive accuracy of 98.24%.

The integration of structured learning, feature extraction techniques, and robust data preprocessing, including class balancing and noise removal, has been instrumental in improving the models' performance. Moreover, the inclusion of explainable AI tools ensures interpretability and fosters trust among clinicians, making these models more viable for practical deployment in clinical settings.

The study also highlights the growing importance of integrating real-time data from wearable devices and expanding datasets to include diverse populations to enhance model generalizability. Addressing challenges such as data privacy, ethical considerations, and computational efficiency will be crucial for future development.

In conclusion, the findings of this study establish the Custom CNN as a benchmark model for heart disease prediction, demonstrating its potential to significantly enhance early diagnosis and treatment planning. With further refinement and real-world integration, these predictive models can play a transformative role in reducing the burden of cardiovascular diseases, improving patient outcomes, and advancing the field of intelligent healthcare systems.

REFERENCES

[1] A. Krizhevsky, I. Sutskever, and G. E. Hinton, "ImageNet classification with deep convolutional neural networks," *Communications of the ACM*, vol. 60, no. 6, pp. 84–90, 2017.

[2] Z. Zhang et al., "Heart disease prediction based on machine learning approaches," *BioMed Research International*, vol. 2017, pp. 1–10, 2017.

[3] J. Schmidhuber, "Deep learning in neural networks: An overview," *Neural Networks*, vol. 61, pp. 85–117, 2015.

[4] P. Rajpurkar et al., "Cardiologist-level arrhythmia detection with convolutional neural networks," *Nature Medicine*, vol. 25, no. 1, pp. 65–69, 2019.

[5] D. P. Kingma and J. Ba, "Adam: A method for stochastic optimization," in *Proceedings of the International Conference on Learning Representations (ICLR)*, San Diego, CA, USA, 2015, pp. 1–15.

[6] C. Chen and T. Guestrin, "XGBoost: A scalable tree boosting system," in *Proceedings of the ACM SIGKDD International Conference on Knowledge Discovery and Data Mining*, San Francisco, CA, USA, 2016, pp. 785–794.

[7] Y. LeCun, Y. Bengio, and G. Hinton, "Deep learning," *Nature*, vol. 521, no. 7553, pp. 436–444, 2015.
[8] A. P. Jawalkar et al., "Early Prediction of Heart Disease with Data Analysis Using Supervised Learning with Stochastic Gradient Boosting," *J. Eng. Appl. Sci.*, vol. 70, no. 122, pp. 1–10, Oct. 2023.
[9] C. Zhou et al., "A Comprehensive Review of Deep Learning-Based Models for Heart Disease Prediction," *Artif. Intell. Rev.*, vol. 57, no. 263, pp. 1–25, Aug. 2024.
[10] N. K. R. Devana, V. R. Sankar Ch, and A. B. Tummala, "A Comprehensive Review on Heart Disease Risk Prediction Using Machine Learning Approaches," *Arch. Comput. Methods Eng.*, vol. 31, no. 10194, pp. 1–20, Sep. 2024.
[11] H. Shin et al., "Deep convolutional neural networks for computer-aided detection: CNN architectures, dataset characteristics, and transfer learning," *IEEE Transactions on Medical Imaging*, vol. 35, no. 5, pp. 1285–1298, May 2016.
[12] T. Hastie, R. Tibshirani, and J. Friedman, *The Elements of Statistical Learning: Data Mining, Inference, and Prediction*, 2nd ed., Springer, 2009.
[13] S. Hochreiter and J. Schmidhuber, "Long short-term memory," *Neural Computation*, vol. 9, no. 8, pp. 1735–1780, 1997.
[14] A. Tiwari, A. Chugh, and A. Sharma, "Ensemble Framework for Cardiovascular Disease Prediction," *arXiv preprint arXiv:2306.09989*, Jun. 2023.
[15] J. Miah et al., "Improving Cardiovascular Disease Prediction Through Comparative Analysis of Machine Learning Models: A Case Study on Myocardial Infarction," *arXiv preprint arXiv:2311.00517*, Nov. 2023.
[16] M. T. García-Ordás et al., "Heart Disease Risk Prediction Using Deep Learning Techniques with Feature Augmentation," *arXiv preprint arXiv:2402.05495*, Feb. 2024.
[17] F. Shishehbori and Z. Awan, "Enhancing Cardiovascular Disease Risk Prediction with Machine Learning Models," *arXiv preprint arXiv:2401.17328*, Jan. 2024.
[18] A. S. Osei-Nkwantabisa and R. Ntumy, "Classification and Prediction of Heart Diseases Using Machine Learning Algorithms," *arXiv preprint arXiv:2409.03697*, Sep. 2024.
[19] H. Li et al., "Advanced Machine Learning Techniques for Early Prediction of Heart Diseases," in *Proc. IEEE Int. Conf. Comput. Intell. Virtual Environ. Human-Centric Comput. (CIVEMSA)*, Nagoya, Japan, 2023, pp. 1–6.
[20] S. R. Pfohl, A. Foryciarz, and N. H. Shah, "An Empirical Characterization of Fair Machine Learning for Clinical Risk Prediction," *J. Biomed. Inform.*, vol. 113, p. 103621, Jan. 2021.
[21] J. Brownlee, *Deep Learning for Time Series Forecasting: Predicting Future with Sequential Data in Python*, Machine Learning Mastery, 2018.
[22] Y. LeCun, Y. Bengio, and G. Hinton, "Deep learning," *Nature*, vol. 521, no. 7553, pp. 436–444, 2015.
[23] S. Hochreiter and J. Schmidhuber, "Long short-term memory," *Neural Computation*, vol. 9, no. 8, pp. 1735–1780, 1997.
[24] K. He, X. Zhang, S. Ren, and J. Sun, "Deep residual learning for image recognition," in *Proc. IEEE Conf. Comput. Vis. Pattern Recognit.*, Las Vegas, NV, USA, 2016, pp. 770–778.
[25] A. Krizhevsky, I. Sutskever, and G. E. Hinton, "ImageNet classification with deep convolutional neural networks," in *Adv. Neural Inf. Process. Syst.*, Lake Tahoe, NV, USA, 2012, pp. 1097–1105.
[26] A. Esteva et al., "A guide to deep learning in healthcare," *Nat. Med.*, vol. 25, no. 1, pp. 24–29, 2019.
[27] L. Breiman, "Random forests," *Mach. Learn.*, vol. 45, no. 1, pp. 5–32, 2001.
[28] C. Chen and T. Guestrin, "XGBoost: A scalable tree boosting system," in *Proc. ACM SIGKDD Int. Conf. Knowl. Discov. Data Mining*, San Francisco, CA, USA, 2016, pp. 785–794.
[29] M. T. Ribeiro, S. Singh, and C. Guestrin, "Why should I trust you? Explaining the predictions of any classifier," in *Proc. ACM SIGKDD Int. Conf. Knowl. Discov. Data Mining*, San Francisco, CA, USA, 2016, pp. 1135–1144.
[30] S. Lundberg and S. Lee, "A unified approach to interpreting model predictions," in *Adv. Neural Inf. Process. Syst.*, Long Beach, CA, USA, 2017, pp. 4768–4777.
[31] G. Litjens et al., "A survey on deep learning in medical image analysis," *Med. Image Anal.*, vol. 42, pp. 60–88, 2017.
[32] P. Rajpurkar et al., "Cardiologist-level arrhythmia detection with convolutional neural networks," *Nat. Med.*, vol. 25, no. 1, pp. 65–69, 2019.

[33] H. Rahman et al., "Machine learning in cardiovascular medicine: Are we there yet?" *Heart*, vol. 106, no. 15, pp. 1157–1161, 2020.
[34] D. Silver et al., "Mastering the game of Go with deep neural networks and tree search," *Nature*, vol. 529, no. 7587, pp. 484–489, 2016.
[35] M. Abadi et al., "TensorFlow: Large-scale machine learning on heterogeneous distributed systems," 2016, [Online]. Available: https://arxiv.org/abs/1603.04467.
[36] F. Chollet, *Deep Learning with Python*, 2nd ed., Manning Publications, 2021.
[37] Z. Zhang et al., "Heart disease prediction based on machine learning approaches," *BioMed. Res. Int.*, vol. 2017, pp. 1–10, 2017.
[38] J. A. Fawcett, "An introduction to ROC analysis," *Pattern Recognit. Lett.*, vol. 27, no. 8, pp. 861–874, 2006.
[39] T. Hastie, R. Tibshirani, and J. Friedman, *The Elements of Statistical Learning: Data Mining, Inference, and Prediction*, 2nd ed., Springer, 2009.
[40] J. Schmidhuber, "Deep learning in neural networks: An overview," *Neural Netw.*, vol. 61, pp. 85–117, 2015.
[41] M. Nielsen, *Neural Networks and Deep Learning*, Determination Press, 2015.
[42] M. R. Karim et al., "Data-level and algorithm-level solutions for imbalanced classification problems: A review," *Int. J. Mach. Learn. Cybern.*, vol. 9, pp. 757–774, 2018.
[43] H. Shin et al., "Deep convolutional neural networks for computer-aided detection: CNN architectures, dataset characteristics, and transfer learning," *IEEE Trans. Med. Imag.*, vol. 35, no. 5, pp. 1285–1298, 2016.
[44] D. P. Kingma and J. Ba, "Adam: A method for stochastic optimization," in *Proc. Int. Conf. Learn. Represent.*, San Diego, CA, USA, 2015, pp. 1–15.
[45] S. Ioffe and C. Szegedy, "Batch normalization: Accelerating deep network training by reducing internal covariate shift," in *Proc. Int. Conf. Mach. Learn.*, Lille, France, 2015, pp. 448–456.
[46] K. Simonyan and A. Zisserman, "Very deep convolutional networks for large-scale image recognition," in *Proc. Int. Conf. Learn. Represent.*, San Diego, CA, USA, 2015.
[47] J. Long, E. Shelhamer, and T. Darrell, "Fully convolutional networks for semantic segmentation," in *Proc. IEEE Conf. Comput. Vis. Pattern Recognit.*, Boston, MA, USA, 2015, pp. 3431–3440.
[48] H. Li et al., "Imbalanced learning for cardiovascular disease prediction," *Appl. Intell.*, vol. 50, no. 8, pp. 2355–2368, 2020.
[49] M. Tan and Q. V. Le, "EfficientNet: Rethinking model scaling for convolutional neural networks," in *Proc. Int. Conf. Mach. Learn.*, Long Beach, CA, USA, 2019, pp. 6105–6114.
[50] J. Deng et al., "ImageNet: A large-scale hierarchical image database," in *Proc. IEEE Conf. Comput. Vis. Pattern Recognit.*, Miami, FL, USA, 2009, pp. 248–255.
[51] T. De Fauw et al., "Clinically applicable deep learning for diagnosis and referral in retinal disease," *Nat. Med.*, vol. 24, no. 9, pp. 1342–1350, 2018.
[52] L. Lu et al., "Artificial intelligence for cardiovascular disease: Past, present, and future," *JACC: Cardiovasc. Imaging*, vol. 13, no. 2, pp. 362–370, 2020.
[53] P. M. Touw et al., "Predictive modeling in clinical settings: Machine learning and logistic regression," *Med. Decis. Making*, vol. 33, no. 5, pp. 572–589, 2013.
[54] E. Soria-Olivas et al., "Handbook of research on machine learning applications and trends," in *Health Informatics Applications*, 2010, pp. 1–15.
[55] R. Dey and F. M. Salemt, "Application of recurrent neural networks in disease classification and prediction," *Neural Netw.*, vol. 123, pp. 219–239, 2020.